MPMI Vol. 38, No. 3, 2025, pp. 365–375, https://doi.org/10.1094/MPMI-08-24-0086-R

RESEARCH

The XopAE Effector from *Xanthomonas phaseoli* pv. *manihotis* Targets HSP20-like p23 Cochaperone to Suppress Plant Basal Immunity

Diana Gómez De La Cruz,[1,2] Darwin A. Castillo,[1] César A. Trujillo B.,[1,2] Cesar A. Medina,[1] Valentina Hurtado-McCormick,[1] Juliana Gil,[3] Meenu Padmanabhan,[4] Silvia Restrepo,[2] Savithramma P. Dinesh-Kumar,[4] Hugo Germain,[5] Camilo López,[3] and Adriana Bernal[1,†]

[1] Laboratory of Molecular Interactions of Agricultural Microbes, LIMMA, Department of Biological Sciences, Universidad de los Andes, Bogotá, Colombia
[2] Laboratory of Mycology and Plant Pathology Uniandes, Department of Biological Sciences, Universidad de los Andes, Bogotá, Colombia
[3] Manihot-Biotec, Department of Biology, Universidad Nacional de Colombia, Bogotá, Colombia
[4] Department of Plant Biology and the Genome Center, College of Biological Sciences, University of California, Davis, CA, U.S.A.
[5] Department of Chemistry, Biochemistry and Physics, Université du Québec à Trois-Rivières, Trois-Rivières, Quebec, Canada

Accepted for publication 14 January 2025.

Pathogenic bacteria use Type 3 effector proteins to manipulate host defenses and alter metabolism to favor their survival and spread. The non-model bacterial pathogen *Xanthomonas phaseoli* pv. *manihotis* (*Xpm*) causes devastating disease in cassava. The molecular role of Type 3 effector proteins from *Xpm* in causing disease is largely unknown. Here, we report that the XopAE effector from *Xpm* suppresses plant defense responses. Our results show that XopAE is a suppressor of basal defenses such as callose deposition and the production of reactive oxygen species. XopAE targets a small heat shock protein (*Me*p23-1 cochaperone) in cassava and its homolog *At*p23-1 in *Arabidopsis*. XopAE localizes to the nucleus and in scattered points throughout the cell border, whereas *Me*p23-1 shows a nucleocytoplasmic localization. Upon interaction, XopAE hijacks *Me*p23-1 to the scattered points throughout the cell border, and they also interact in the nucleus. Our results indicate that the interaction between XopAE and *Me*p23-1 is essential for suppressing basal plant defense. This study is one of the first to address the molecular mechanisms deployed by *Xpm* to cause disease in cassava, a non-model crop plant.

Keywords: cassava, suppression of immunity, type 3 effectors, *Xanthomonas*

[†]Corresponding author: A. Bernal; abernal@uniandes.edu.co

D. Gómez De La Cruz and D. A. Castillo contributed equally to the manuscript.

Author contributions: D.G.D.L.C., C.A.T.B., D.A.C., C.A.M., V.H.-M., J.G., M.P., and A.B. carried out the experiments. D.G.D.L.C. and C.A.T.B. wrote the first draft. D.A.C. wrote the last manuscript draft for journal submission. All the authors read and made comments on the final manuscript. A.B., S.R., C.L., and H.G. helped supervise the project. D.G.D.L.C., C.A.T.B., and A.B. conceived the original idea. A.B., S.P.D.-K., M.P., H.G., and C.L. secured the funds to carry out the experiments. A.B. supervised and administered the project.

Funding: This research was funded by the Colombian Ministry of Science (Minciencias, former Administrative Department for the Advancement of Sciences, contract no. 0794-2013) and the Faculty of Sciences and Vice Dean of Research office at the Universidad de los Andes for funding given to A. Bernal (INV-2023-162-2847). H. Germain was supported by the Canadian Network for Research and Innovation in Machining Technology, Natural Sciences and Engineering Research Council of Canada (RGPIN-2020-04002). The Faculty of Sciences at the Universidad de los Andes (project INV-2022-143-2515) and Mitacs Globalink (ref. FR95202) financed D. A. Castillo for a research internship in Canada.

***e*-Xtra:** Supplementary material is available online.

The author(s) declare no conflict of interest.

Plants are constantly threatened by pathogen attacks, which can result in either the establishment or restriction of disease. Co-evolution with pathogens has shaped a two-tiered plant immune system that perceives biotic threats and triggers the corresponding defense responses. The first tier recognizes pathogens by identifying highly conserved microbial molecules known as microbe-associated molecular patterns (or pathogen-associated molecular patterns [PAMPs]) (Boller 1995; Dangl et al. 2013; Jones and Dangl 2006; Ngou et al. 2022; Wang et al. 2020; Zipfel and Robatzek 2010). Diverse PAMPs, such as fungal chitin, bacterial lipopolysaccharides, ergosterol, bacterial elongation factor Tu, and flagellin, are recognized by pattern-recognition receptors, inducing pattern-triggered immunity (PTI) (Bittel and Robatzek 2007; Boutrot and Zipfel 2017; Dangl et al. 2013; Dow et al. 2000; Jones and Dangl 2006; Ngou et al. 2022; Nicaise et al. 2009; Zipfel 2009). PTI results in the activation of several processes associated with plant defense, including plant cell wall strengthening, generation of reactive oxygen species (ROS), callose deposition, activation of mitogen-activated protein kinase cascades, and the synthesis of antimicrobial compounds, which collectively contribute to

restricting the establishment and growth of the pathogen within the plant tissue (Boller and Felix 2009; Bolton 2009; Felix et al. 1999; Zipfel 2009; Zipfel et al. 2004).

The second tier is the perception of pathogens by the recognition of pathogen-encoded virulence factors called effector proteins. In the case of gram-negative pathogenic bacteria, these proteins are translocated from the bacterial cytoplasm into the plant cells through a molecular syringe known as the type three secretion system (T3SS). These effector proteins, or type three effectors (T3Es), contribute to pathogen fitness and plant defense suppression, favoring survival and multiplication (Galán and Collmer 1999; Hueck 1998). However, plants can specifically recognize effectors through intracellular nucleotide binding site-leucine-rich repeat (NLR) class receptors, which leads to the activation of the second tier of plant defense, known as effector-triggered immunity (ETI) (Cui et al. 2015; Flor 1971; Jones and Dangl 2006; Ngou et al. 2022). The responses in ETI tend to be more intense and prolonged than in PTI. ETI commonly leads to a hypersensitive response (HR), a form of localized programmed cell death that restricts the spread of the pathogen (Dodds and Rathjen 2010). However, emerging evidence suggests that PTI and ETI share signaling mechanisms, which can be mutually potentiated to fence off the pathogen's attack (Ngou et al. 2021, 2022). Disease can therefore occur when plants fail to detect pathogens or when pathogens successfully suppress PTI and/or ETI.

Several T3Es have been described in the genus *Xanthomonas*, and determining their role as suppressors of PTI and ETI in plant defenses is a crucial step in understanding the development of plant diseases. Among the diverse T3Es within the genus are the *Xanthomonas* outer proteins (Xop) (Gómez-Cano et al. 2019; Ryan et al. 2011; Timilsina et al. 2020; White et al. 2009; Zárate-Chaves et al. 2021a). Xop effectors act as modulators of plant metabolism, as well as of PTI and ETI in several model plants, and different approaches have been used to understand the role of Xop effectors in the suppression of plant defenses and to determine their targets in host plants (Arrieta-Ortiz et al. 2013; Kay and Bonas 2009; Medina et al. 2018; Üstün and Börnke 2014; White et al. 2009; Zárate-Chaves et al. 2021a).

The most poorly understood Xop effectors are those from non-model systems, such as *Xanthomonas phaseoli* pv. *manihotis* (*Xpm*), the causal agent of bacterial blight in cassava (*Manihot esculenta* Crantz) and the most important bacterial disease affecting this crop (Boher and Verdier 1994; Lozano 1986; Verdier et al. 2004; Zárate-Chaves et al. 2021a). Depending on environmental conditions, *Xpm* causes yield losses that range between 30 and 100% (Timilsina et al. 2020; Zárate-Chaves et al. 2021a). *Xpm* lives as an epiphyte and enters leaves through natural openings and wounds. Once inside, *Xpm* multiplies in the mesophyll, reaches the vascular tissue, and moves systemically in the plant (Zárate-Chaves et al. 2021a). Therefore, this pathogen can induce symptoms such as angular leaf spots, blight, stem cankers, gum exudates, and plant death (Zárate-Chaves et al. 2021a). Previous efforts to describe cassava bacterial blight have focused on population genetic studies (Arrieta-Ortiz et al. 2013; Bart et al. 2012; Botero et al. 2020; Gómez-Cano et al. 2019; Zárate-Chaves et al. 2021b) and pathogen detection (Bernal-Galeano et al. 2018; Flores et al. 2019) rather than mechanistic approaches to understand the involvement of Xop effectors during disease at a molecular level.

XopAE is a highly conserved T3E within *Xpm* populations. It is catalogued as one of the nine core effectors among *Xpm* strains; its sequence varies very little among strains worldwide (Arrieta-Ortiz et al. 2013; Bart et al. 2012) and is adjacent to the cluster encoding the T3SS in the genome of *Xpm* reference strain CIO151 (Arrieta-Ortiz et al. 2013). XopAE contains a leucine-rich repeat (LRR) domain (Kim et al. 2003), a structural component of pattern-recognition receptors and NLRs in plants that is essential for the recognition of pathogens from different kingdoms (Caplan et al. 2008; Eitas and Dangl 2010; McHale et al. 2006). Interestingly, effectors from *X. euvesicatoria* (*Xeu*), such as XopL, also contain an LRR domain, which is essential for protein-protein interactions with its host targets for suppression of PAMP-elicited gene expression. The LRR portion of XopL is required for programmed cell death elicitation in the host plant, but it is dispensable for the ubiquitin ligase activity (Singer et al. 2013). XopAE was previously described as a suppressor of PTI-related responses in *Xeu*, probably through an E3 ubiquitin ligase activity (Popov et al. 2016, 2018). However, the XopAE of *Xeu*, reported as a PTI suppressor (Popov et al. 2016), is encoded in a locus split into two open reading frames (ORFs) (HpaF and a truncated XopAE; Supplementary Fig. S1) by a frameshift mutation, and the XopAE segment has been further characterized, revealing the E3 ubiquitin ligase activity of this effector (Popov et al. 2018). Despite the role of XopAE as a suppressor of PTI, its targets in host plants have yet to be identified. To elucidate the role of XopAE from *Xpm* during the development of cassava bacterial blight disease, we evaluated the potential involvement of this T3E as a plant defense suppressor using heterologous systems. Our findings reveal that XopAE suppresses PTI but not ETI responses. We also identified a XopAE target in cassava, an HSP20-like p23 protein, and show its role in plant defense. Our results suggest that XopAE interaction with the host protein p23 is crucial for inhibition of plant defense. This study is the first molecular characterization of a Xop effector from *Xpm* targeting a protein in its native host, cassava.

Results

XopAE suppresses PTI but not ETI in non-host plants

To determine if XopAE can suppress PTI, we used the engineered nonpathogenic bacterium *P. fluorescens* to deliver XopAE (NCBI accession no. RWU20036) into plant cells. *P. fluorescens* naturally elicits PAMP responses in *A. thaliana.* The engineered strain, carrying pML123, expresses the functional T3SS from the plant-pathogenic bacterium *P. syringae* and is able to deliver bacterial effectors into plant cells (Guo et al. 2009). As expected, when *A. thaliana* Col-0 plants were inoculated with the *P. fluorescens* strain with T3SS (*Pf*::T3SS), the number of callose deposits was higher than in mock-treated plants (Fig. 1A). In contrast, the callose deposit count was significantly lower when plants were inoculated with *P. fluorescens* carrying XopAE (*Pf*::XopAE) (Fig. 1A), and they were comparable to those inoculated with *P. fluorescens* carrying *XopN* (*Pf*::XopN), which we had previously reported (Medina et al. 2018). We next tested XopAE's impact on ROS induced during PTI. For this, we infiltrated *Pf*::T3SS and *Pf*::XopAE strains into *Nicotiana tabacum* leaves, and ROS levels were measured. The ROS burst was lower in plants inoculated with *Pf*::XopAE compared with plants inoculated with the *Pf*::T3SS control strain (Fig. 1B; Supplementary Fig. S2). These results indicate that XopAE can suppress typical PTI responses such as callose deposition and ROS burst.

We next tested whether XopAE also suppresses ETI. For this, we used *P. fluorescens* (pHIR11) expressing the HopA1 T3E from *P. syringae* pv. *tomato* (*Pf*::HopA1), which is recognized by tobacco plants and induces HR (Alfano et al. 1997). To test whether XopAE can suppress HR induced by HopA1, we co-infiltrated different concentrations of *Pf*::HopA1 mixed with *Pf*::XopAE and *Pf*::HopA1 alone into tobacco leaves. No differences in HR were observed between infiltration spots with *Pf*::HopA1 alone or co-infiltrated with *Pf*::XopAE (Fig. 1C), indicating that XopAE cannot suppress HR induced by HopA1 in tobacco.

XopAE interacts with a small heat shock protein (sHSP)

To explore the molecular mechanisms of action of XopAE in planta, a yeast two-hybrid screen was conducted using XopAE as the bait and a complementary DNA (cDNA) library from cassava variety SG107-35 infected with *Xpm* (González Almario and López Carrascal 2008) as the prey. One of the identified XopAE-interacting proteins is an sHSP, specifically an HSP20-like protein (locus name: cassava4.1_017133m.g [also Manes.01G217800]; http://www.phytozome.net/), described as a p23 cochaperone in *A. thaliana*. This interactor, hereafter referred to as *Me*p23-1, contains a CS (CHORD-containing protein and SGT1) domain that is present in eukaryotic cochaperone proteins such as SGT1(suppressor of the G2 allele of skp1) that play an important role in plant defense (Austin et al. 2002).

To further confirm the interaction between XopAE and *Me*p23-1, a targeted yeast two-hybrid assay was performed using BD:XopAE and AD::*Me*p23-1, and vice versa (AD::XopAE and BD::*Me*p23-1). The yeast strains co-transformed with *Me*p23-1 and XopAE could grow in the triple dropout selective medium (SD -L-W-H) (Fig. 2A), indicating that XopAE interacts with cassava p23-1. No yeast growth was observed in the selective medium (SD -L-W-H) when each construct was co-transformed with the corresponding empty vector (Fig. 2A), indicating that none of the proteins is auto-active in the yeast two-hybrid system. Interestingly, we observed a positive interaction when yeasts were transformed with plasmid constructs expressing the *Me*p23-1 fused to BD or AD domains (Fig. 2A), suggesting that cassava p23 can form homodimers.

Furthermore, the interaction between XopAE and *Me*p23-1 was verified in an in-planta co-immunoprecipitation assay. For this, *Me*p23-1 fused to the 3×Myc tag and XopAE fused to the 3×HA tag were transiently expressed in *N. benthamiana*

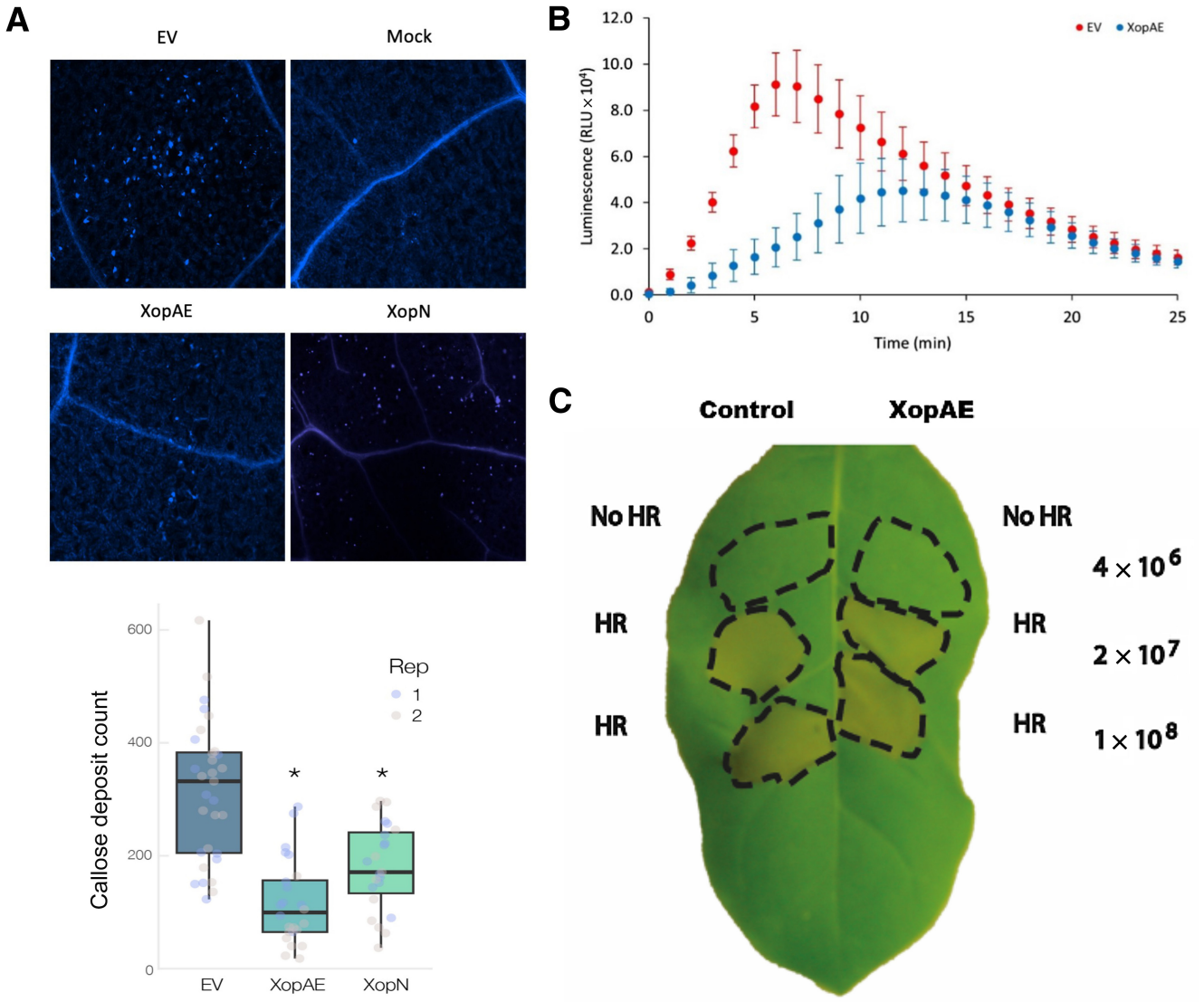

Fig. 1. XopAE suppresses pattern-triggered immunity but not effector-triggered immunity responses in non-host plants. **A,** Representative images of callose deposition in *Arabidopsis thaliana* Col-0 leaves infiltrated with *Pseudomonas fluorescens* (pLN1965) carrying a type three secretion system (*Pf*::T3SS) or XopAE (*Pf*::XopAE) and XopN (*Pf*::XopN). Mock infiltration with morpholine ethane sulfonic acid buffer was used as the negative control (Mock). Results represent 10 examined spots from each of three independent plants. This experiment was repeated five times with similar results. EV, empty vector. **B,** Suppression of reactive oxygen species (ROS) production by XopAE. *Pf*::T3SS and *Pf*::XopAE were infiltrated in *Nicotiana tabacum* cultivar Xanthi leaves, and ROS production was measured over time. Error bars represent 95% confidence intervals. RLU, relative light units. **C,** Hypersensitive response (HR) suppression assay. *N. tabacum* cultivar Xanthi leaves were infiltrated with different amounts of a mixture of *Pf*::HopA1 plus *Pf*::pLN1965 (left) and a mixture of *Pf*::HopA1 plus *Pf*::pLN1965 (XopAE) (right). HR responses were visualized at 24 h postinfiltration. The strain *P. fluorescens* (pHIR11) carrying pML123 was used as a positive control for HR elicitation, as it holds a T3SS and the effector HopA1 from *P. syringae* pv. *syringae*, which is recognized in *N. tabacum* cultivar Xanthi. This strain was mixed with *P. fluorescens* (pLN1965) carrying pLN615:XopAE. This experiment was repeated three times with similar results.

leaves. XopN fused to 3×HA was used as a control. XopAE but not XopN co-immunoprecipitated with *Me*p23-1 (Fig. 2B). These results indicate that *Me*p23-1 specifically interacts with XopAE in vivo.

Subcellular localization and in planta interaction of *Me*p23-1 and XopAE

To better understand the interaction in planta between *Me*p23-1 and XopAE, we first determined the subcellular localization of these proteins. XopAE was fused to citrine and expressed under the control of the constitutive 35S promoter in *N. benthamiana* leaves using *Agrobacterium*-mediated transient expression. After 30 h, XopAE was observed to localize to the nucleus and punctate sites throughout the cell border (Fig. 2C; Supplementary Fig. S3). *Me*p23-1 fused to citrine, on the other hand, localized to the cytoplasm and the nucleus (Fig. 2C). To determine the subcellular site of interaction between XopAE and *Me*p23-1, we performed a noninvasive bimolecular fluorescence complementation (BiFC) assay (Kerppola 2008). For this, we transiently co-expressed XopAE::^{C}Citrine and *Me*p23-1::^{N}Citrine fusions under the control of the constitutive 35S promoter (Padmanabhan et al. 2013). The citrine fluorescence was only reconstituted when both XopAE and *Me*p23-1 were present, and the fluorescence was observed in the nucleus and in the punctate sites through the cell border (Fig. 2D; Supplementary Fig. S4). No citrine fluorescence was

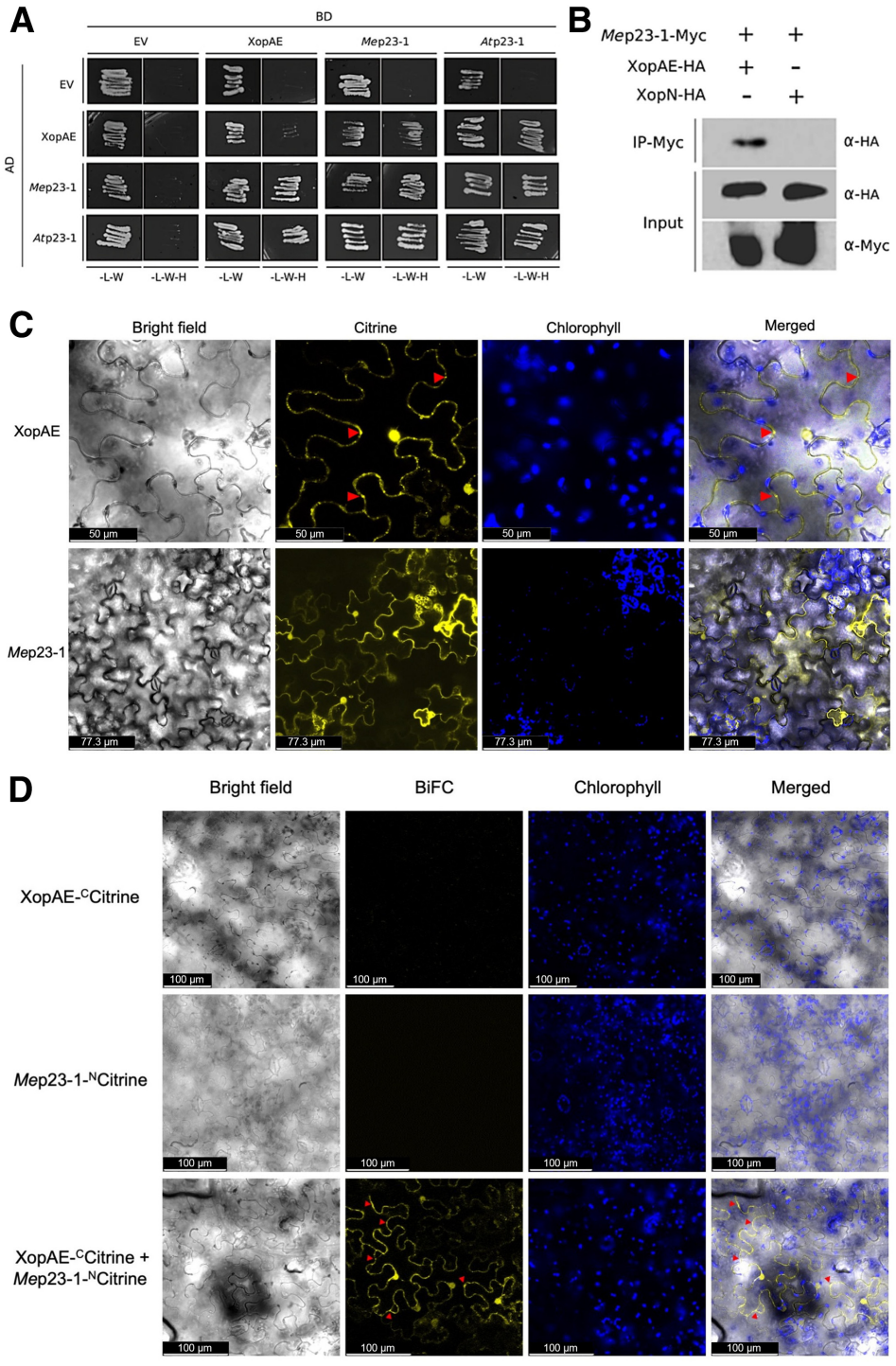

Fig. 2. XopAE interacts with an HSP20-like p23 cochaperone. **A,** Growth of yeast strains co-expressing *Me*p23-1 or *At*p23-1 fused to the GAL4 DNA binding domain (BD) and XopAE fused to the GAL4 activation domain (AD), and vice versa, on control media lacking leucine and tryptophan (-L-W) and selective media lacking leucine, tryptophan, and histidine (-L-W-H). Self-interaction of *Me*p23-1 and *At*p23-1 was tested by co-expressing the same protein fused to the AD and BD in the same yeast strain. EV, empty vector. **B,** XopAE co-immunoprecipitates with *Me*p23-1. XopAE-3×HA and *Me*p23-1-3×Myc were transiently expressed in *Nicotiana benthamiana*. Proteins were extracted and subjected to immunoprecipitation with α-Myc and detected with α-HA antibodies. XopN was used as a negative control. HA, hemagglutinin. **C,** Confocal images of *N. benthamiana* epidermal leaf cells transiently expressing XopAE-Citrine at 30 h postinoculation (hpi) (second column, top) and *Me*p23-1-Citrine at 48 hpi (second column, bottom). The chlorophyll autofluorescence was used to mark the chloroplasts (third column). Bright-field (first column) and merged (fourth column) images are shown. Red arrowheads indicate the puncta where XopAE localizes. This experiment was repeated three times with similar results. **D,** XopAE-^{C}Citrine or *Me*p23-1-^{N}Citrine alone or together expressed transiently in *N. benthamiana* leaves. Citrine fluorescence is reconstituted in cells co-expressing XopAE-^{C}Citrine and *Me*p23-1-^{N}Citrine (second column, bottom panel) but not when XopAE-^{C}Citrine (second column, top panel) or *Me*p23-1-^{N}Citrine (second column, middle panel) expressed alone at 30 hpi. The chlorophyll autofluorescence was used to mark the chloroplasts (third column). Bright-field (first column) and merged (fourth column) images are shown. Red arrowheads indicate the puncta where XopAE co-localizes with *Me*p23-1. This experiment was repeated three times with similar results. BiFC, bimolecular fluorescence complementation.

observed when XopAE or *Me*p23-1 was expressed alone. These results indicate that XopAE and *Me*p23-1 both localize to the nucleus, but XopAE also localizes to the punctate structures and *Me*p23-1 localizes to the cytoplasm. XopAE interacts with *Me*p23-1 in the nucleus and punctate structures.

XopAE targets the CS domain of *Me*p23-1

We next sought to identify the role of the highly conserved KVDWDKWVDED motif of p23-1 cochaperones in protein-protein interaction (Zhang et al. 2010). To this end, we predicted the 3D structures of *Me*p23-1 and XopAE. We used these structures to simulate the XopAE- *Me*p23-1 interaction using the protein-protein docking tool of MOE software. From the 100 docked poses generated by MOE (Supplementary Fig. S5A), we selected the best one (Supplementary Fig. S5A and B) for epitope analysis. The epitope analysis predicted that XopAE binds to seven amino acids (Met1, Lys84, Trp86, Trp87, Lys88, Trp105, and Asp106) of *Me*p23-1 (Fig. 3B). It is suggestive that most of the predicted interacting residues relay in the N-terminus of *Me*p23-1, and W105 and D106 belong to the highly conserved motif among p23-1 cochaperones. Thus, we posit that the C-terminal region and CS motif of p23-1 cochaperones are essential for their interaction with other proteins and might be a target of XopAE and other T3Es from plant pathogens.

The *Me*p23-1 homolog is important for basal defense in *Arabidopsis*

Because XopAE interacts with *Me*p23-1 and contains a CS domain that is present in other cochaperones that play a role in plant defense, including SGT1 (Austin et al. 2002), we were interested in determining whether *Me*p23-1 is involved in plant immunity. Given the lack of mutant resources in cassava and the time-consuming and laborious effort to generate knockout or RNA interference transgenic plants in this species, we attempted to evaluate the importance of *Me*p23-1 in plant defense in the *A. thaliana* model system. For this, a reciprocal tblastn using the *Me*p23-1 protein sequence was used to identify a putative ortholog in *A. thaliana*. This gene has been reported as *Atp23-1* (AT4G02450) and encodes a p23 cochaperone protein. *At*p23-1 and *Me*p23-1 proteins share 83% similarity at the CS domain in the N-terminus and have an overall identity of 46%. In contrast, they differ at the C-terminus, mainly due to 17 MGG repeats present in *At*p23-1 (Fig. 3A).

To support the use of the *A. thaliana* heterologous system for assays with XopAE from *Xpm*, we confirmed that XopAE interacts with *At*p23-1 in the yeast two-hybrid assay (Fig. 2A). Furthermore, similar to *Me*p23-1, *At*p23-1 can also interact with itself in the yeast two-hybrid system (Fig. 2A). These results support a possible functional homology between *Me*p23-1 and *At*p23-1. To test the function of *At*p23-1 in plant defense, we obtained an *Arabidopsis* insertional transfer DNA (T-DNA) mutant line for this gene (SAIL_245_H06) from the Arabidopsis Biological Resource Center and named it *atp23-1*. We performed callose deposition assays in the *atp23-1* mutant line and in Col-0 wild-type plants to assess the role of *Atp23-1* in basal plant defense. For this, we infiltrated *A. thaliana* leaves with *Pf*::T3SS and compared the amount of callose deposits between plant genotypes. *p23-1* T-DNA mutant plants showed a significantly decreased callose deposit count compared with Col-0 plants when inoculated with *Pf*::T3SS. To further evaluate the role of p23-1, we generated stable transgenic plants expressing *At*p23-1 in the *p23-1* mutant background (*p23-1*::35S:*At*p23-1). There was no significant difference in callose deposition between *p23-1*::35S:*At*p23-1 and Col-0 wild-type plants (Fig. 4), indicating successful complementation of the phenotype. These results indicate that *At*p23-1 acts as a positive regulator of PTI in *A. thaliana*, as the *Atp23-1* mutant genetic background has an impaired callose deposition response. To determine whether *Me*p23-1 is also involved in PTI, we generated a transgenic *Me*p23-1 overexpression line in the *Atp23-1* mutant background. The callose deposition upon infiltration with *Pf*::T3SS in *Atp23-1*::35S:*Me*p23-1 was comparable to that in Col-0 and in *Atp23-1*::35S:*Atp23-1* (Fig. 4). Taken together, these results indicate functional homology between *At*p23-1 and *Me*p23-1, confirming the role of *Me*p23-1 in basal defense.

*At*p23-1 is required for the PTI suppression activity of XopAE in *Arabidopsis*

We next determined whether a functional *At*p23-1 is required for the PTI suppression activity of XopAE. For this, we infiltrated *atp23-1* mutant and Col-0 wild type plants with *Pf*::XopAE. In the *Atp23-1* mutant background, we observed increased callose deposition upon infiltration with *Pf*::XopAE compared with Col-0, *p23-1*::35S:*At*p23-1, or *p23-1*::35S:*Me*p23-1 plants (Fig. 4). In Col-0, we observed reduction in callose deposits upon infiltration with *Pf*::XopAE compared with *Pf*::T3SS (Fig. 4) as expected based on the PTI suppression activity of XopAE. To test whether suppression of callose deposition is specifically mediated by XopAE, *atp23-1*, Col-0, *p23-1*::35S:*At*p23-1, or *p23-1*::35S:*Me*p23-1 plants were inoculated with *Pf* expressing the T3E effector XopAO1 from *Xpm*. Pf0::XopAO1 inhibited callose deposition in all four tested plant lines (Fig. 4), regardless of their genotype. These results confirm that the functional *At*p23-1 and *Me*p23-1 are specifically required for XopAE-mediated suppression of PTI response.

Discussion

Xpm causes significant losses in cassava, affecting people who rely on this plant as a main source of food and income (Zárate-Chaves et al. 2021a). Despite the importance of cassava, there are scarce resources available for the study of candidate genes using reverse genetics in this plant. Hence, using heterologous systems that allow for evaluating gene function is useful for the study of the *Xpm*-cassava pathosystem. The T3Es from *Xanthomonas* are proteins involved in nutrient acquisition and suppression of defenses in various host plants (Timilsina et al. 2020; White et al. 2009). So far, there are only two reports elucidating the involvement of Xop effectors from *Xpm* in virulence and suppression of plant immunity (Medina et al. 2018; Mutka et al. 2016). In this study, we report the role of the effector XopAE in suppression of basal plant defenses. Using the *A. thaliana-P. fluorescens* system, which has been previously used to demonstrate the role of *Xpm* T3Es in virulence and immune response suppression (Medina et al. 2018), we showed that XopAE suppresses PTI responses such as callose deposition and ROS production but not HopA1-mediated ETI in tobacco. Previously, XopAE from *Xeu* has been shown to inhibit flg22-induced gene expression and to suppress callose deposition in *A. thaliana* and enhance disease symptoms in tomato plants (Popov et al. 2016). Because PTI responses are conserved across plants, our results showing that XopAE can suppress PTI in *Arabidopsis* suggest that XopAE can also suppress PTI in cassava.

We showed that XopAE directly interacts with the sHSP *Me*p23-1 from cassava in yeast two-hybrid, co-immunoprecipitation, and BiFC assays. XopAE can also target the *Me*p23-1 homologue in *Arabidopsis At*p23-1, which is a HSP20-like cochaperone protein, known to bind HSP90-client complexes and stabilize them through the N-terminal CS domain (Garcia-Ranea et al. 2002; Li et al. 2015). The CS domain is highly conserved in *Me*p23-1 and is characterized by the presence of an antiparallel β-sandwich fold formed by several β-strands, which is required for binding to HSP90 in an ATP-dependent manner in *Arabidopsis* (Garcia-Ranea et al. 2002;

Lambert et al. 2011; Li et al. 2015). p23 homologs from various plants share high identity, and their N-terminal region is highly conserved, as shown for *At*p23-1 and *Me*p23-1. The amino acid sequence KVDWDKWVDED following the CS domain (residues 102 to 112) remains invariant among plant p23 cochaperones. The highest divergence between *At*p23-1 and *Me*p23-1 is found at the C-terminus due to the presence of an MGG repeat segment in the *At*p23-1 protein, which is absent in *Me*p23-1. This glycine-rich region is not essential for binding to HSP90, and it may therefore not dictate the role of *At*p23-1 (Forafonov et al. 2008; Johnson et al. 2007). As previously reported for the human p23 cochaperone and many plant sHSPs (Guo et al. 2020;

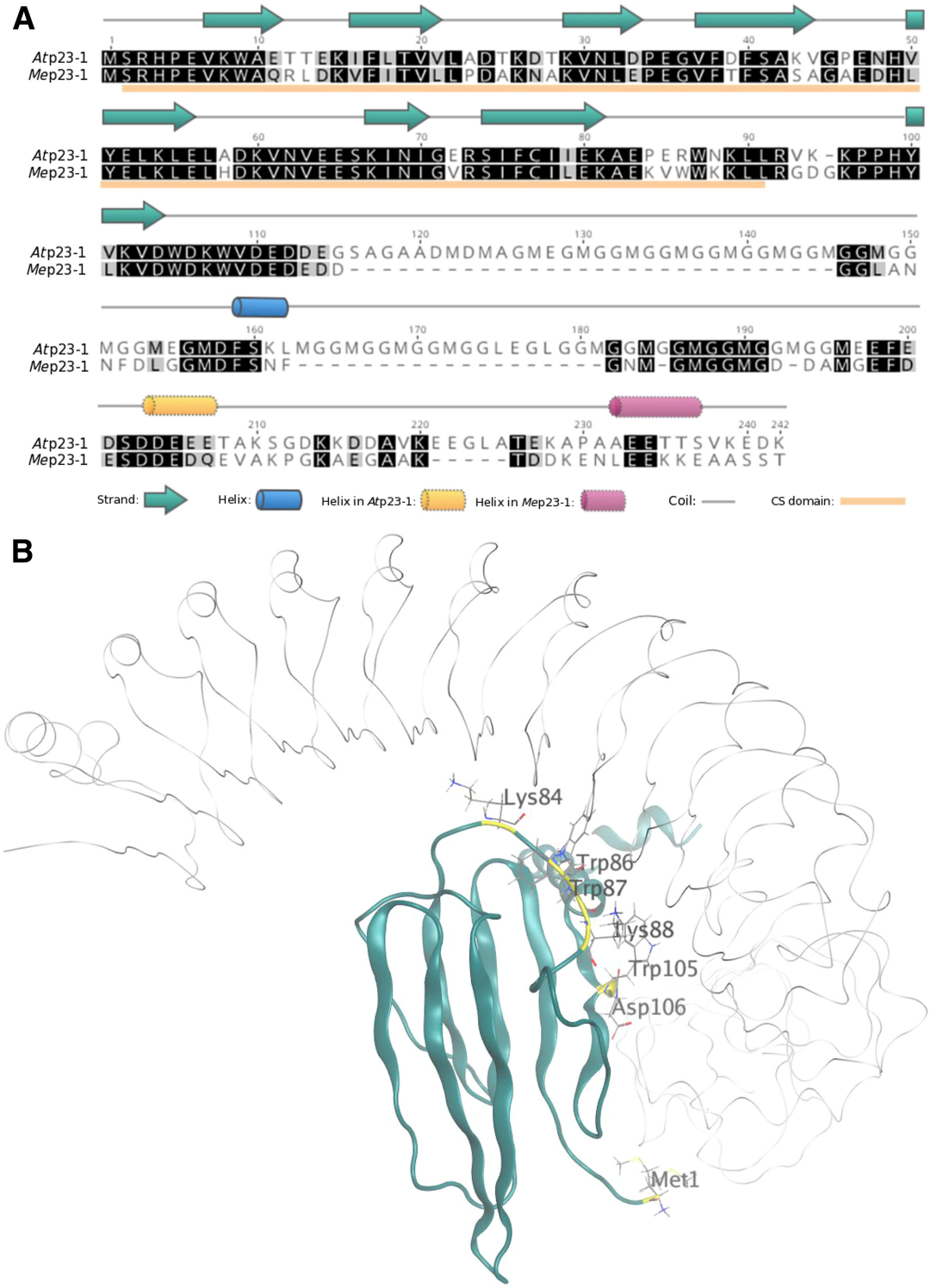

Fig. 3. **A,** Protein structure prediction and molecular docking simulations suggest that the XopAE leucine-rich repeat domain binds to the N-terminus of *Me*p23-1. Alignment of *At*p23-1 (AT4G02450.1) and *Me*p23-1 (cassava4.1_017133m.g) amino acids. Prediction of the secondary structures according to PSIPRED is shown above the amino acid alignment. Black shaded regions include identical residues. **B,** Ribbon of XopAE-*Me*p23-1 interaction. XopAE is colored gray, and *Me*p23-1 is colored green. The epitope analysis indicates that in the best cluster of interactions (score: −9.58), XopAE binds to the Met1, Lys84, Trp86, Trp87, Lys88, Trp105, and Asp106 residues of *Me*p23-1 (highlighted in yellow).

Santhanagopalan et al. 2018), we found that *Me*p23-1 and *At*p23-1 can form homodimers. However, the function and biological relevance of the formation of dimers or complexes of higher molecular order require further investigation.

Whereas XopAE localizes to the nucleus and punctate structures, *Me*p23-1 localizes to the nucleus and the cytoplasm, like the localization reported for its homologue in *Arabidopsis At*p23-1 (D'Alessandro 2013; Tosoni et al. 2011). When both XopAE and *Me*p23-1 are co-expressed, XopAE seems to hijack *Me*p23-1 to the punctate structures and to the nucleus, where they interact. However, we cannot distinguish whether these punctate structures are in the cytosol or in the plasma membrane. It has been shown that HSPs can form granules when plants experience abiotic stress, but little is known about the participation of those structures in responses to biotic stress (Maruri-López et al. 2021). One report showed that the viral RNA-dependent RNA polymerase from the rice stripe virus interacts with the sHSP HSP20 from rice and its ortholog in *N. benthamiana*. In addition, RNA-dependent RNA polymerase modifies the subcellular localization of those HSPs by inhibiting the formation of sHSP granules (Li et al. 2015). We cannot affirm that the punctates where XopAE localizes are sHSp granules, but the XopAE-*Me*p23-1 in vivo interaction evidenced an apparent hijacking that may be relevant for the PTI suppression by XopAE.

Our results indicate that the *atp23-1* mutant shows low callose deposition, a sign of impaired basal plant immune responses. Subsequent trans-complementation of mutant plants with *Me*p23-1 confirmed the involvement of this protein in responses related to PTI, such as cell wall thickening through callose papillae. We hypothesize that p23-1 might have a role in stabilizing protein complexes involved in either the direct synthesis of callose deposition or in signaling processes that lead to basal immune responses. The SGT1 protein involved in plant defense responses shares the CS domain of p23 cochaperones and associates with HSP90. SGT1 is required for disease resistance triggered by a range of NLR proteins in diverse plants,

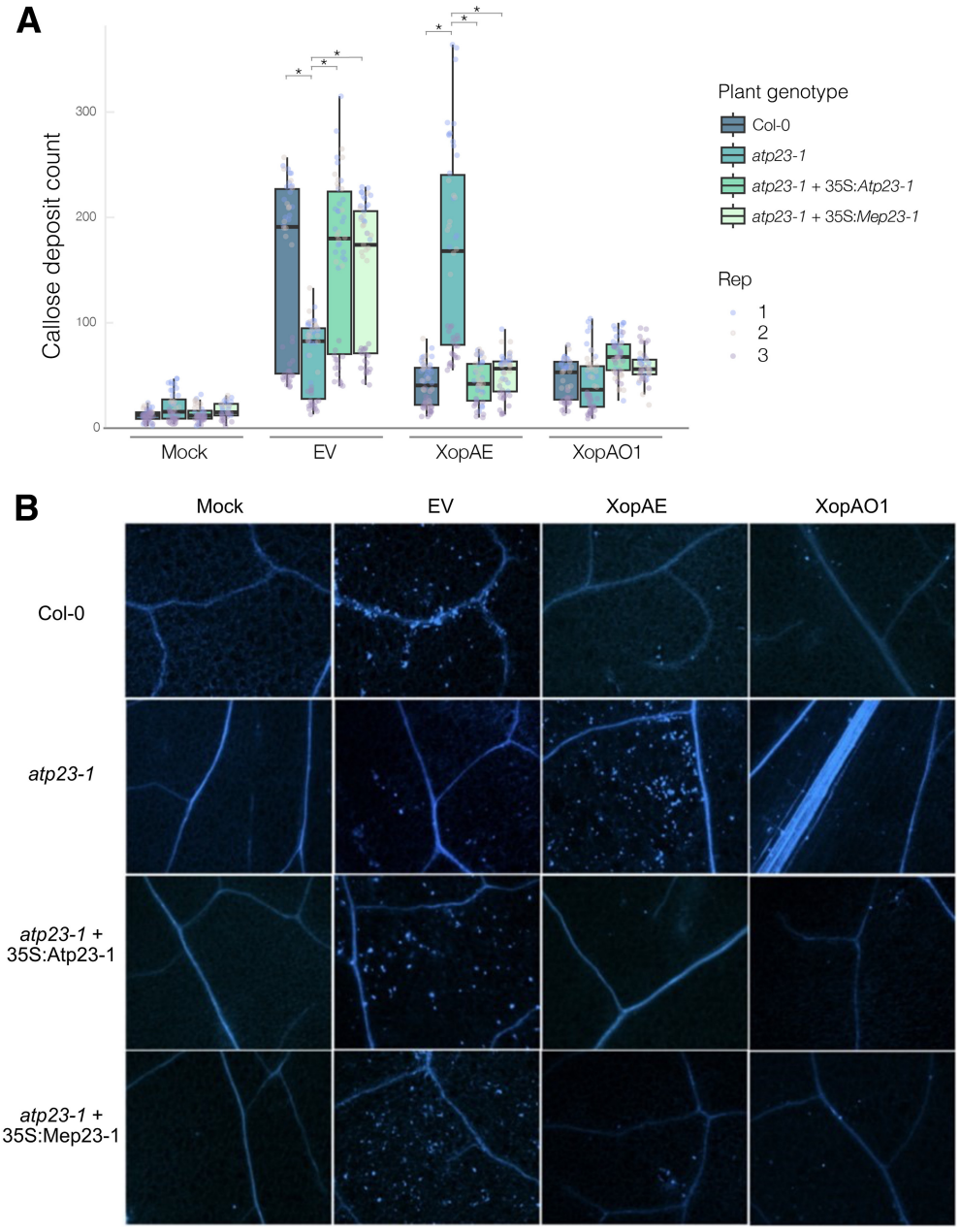

Fig. 4. *At*p23-1 and *Me*p23-1 function in pattern-triggered immunity responses. **A,** Quantitative analysis of callose deposits per analyzed field. Different *Arabidopsis thaliana* plants infiltrated with *Pf*::T3SS, *Pf*::XopAE, or *Pf*::XopAO1 were infiltrated onto Col-0, *atp23-1*, *atp23-1*::*Atp23-1*, and *atp23-1*::*Mep23-1*, and callose deposition was quantified at 16 h postinoculation. Mock infiltration with morpholine ethane sulfonic acid was used as a negative control. At least eight fields were observed per leaf, and three leaves were analyzed per treatment. Experiments were repeated at least twice. A nonparametric Kruskal-Wallis test ($P < 0.05$) was performed to determine significant differences. An asterisk (*) corresponds to significantly different treatments based on Dunnett's test ($\alpha < 0.05$). **B,** Representative images of callose deposition. EV, empty vector.

such as *Arabidopsis*, barley, and *N. benthamiana*, in complex with RAR1 and HSP90 (Austin et al. 2002). Silencing HSP18 in a resistant rice variety increased its susceptibility to *X. oryzae* pv. *oryzae*, and overexpression of this gene significantly enhanced resistance in a susceptible accession (Kuang et al. 2017). Strong evidence shows that sHSPs play essential roles in response to biotic stress in plants. It is reasonable to conclude that sHSPs are conserved targets of effector proteins from different pathogens, as in the XopAE and *Me*p23-1 interaction. Nevertheless, the finely tuned interplay between hormone regulation, signal transduction, development, and immunity can also link p23-1 to plant defense.

It has been reported that HSP90 and RAR1 bind to the small GTPase Rac1 to promote ROS accumulation in response to pathogens (Thao et al. 2007). We hypothesize that XopAE might associate with *Me*p23-1 to prevent it from forming a complex with HSP90, thereby affecting the processes in which such complex is involved, namely folding, stabilization, or activating signaling proteins involved in the induction of defense responses (Felts and Toft 2003; Pearl and Prodromou 2006). XopAE might interfere with the HSP90 complex, explaining its ability to suppress ROS bursts in tobacco. Surprisingly, without a functional p23-1 cochaperone, XopAE cannot suppress callose deposition, which suggests a dual role of p23-1 in plant immunity and indicates the XopAE requirement of a functional host target for its ability to suppress basal host defense. Intriguingly, although XopAE might target the HSP90 complex required for R protein accumulation via p23-1, it was not shown to suppress ETI responses triggered by the recognition of HopA1 in tobacco. However, we cannot rule out the possibility that XopAE affects the stabilization of other R proteins in cassava, thereby promoting disease.

Conclusion

The control of cassava bacterial blight caused by *Xpm* relies on improving sanitary agricultural practices. There must be adequate and sustainable strategies to control and eradicate the problem. Thus, generating resistant varieties based on *R* genes is the most efficient strategy to tackle disease incidence. Nonetheless, little is known about *R* genes recognizing *Xpm* T3Es in cassava. The HSP90 complex is required to stabilize and accumulate several R proteins. It is still unknown whether the same occurs in cassava. Recent transcriptome analysis in a cassava variety resistant to cassava brown streak disease showed that the expression of HSPs, chaperone proteins, and NLR proteins is synchronized during infection (Anjanappa et al. 2018), suggesting a synergistic relationship between these proteins to confer a resistance phenotype. Here, we found that XopAE, a core *Xpm* T3E, suppresses plant defenses, most likely by targeting an HSP20-like chaperone protein. Hence, our research is an essential step toward understanding the molecular interaction between *Xpm* and cassava, thus providing relevant information for developing effective, durable resistance to cassava bacterial blight.

Materials and Methods

Bacterial and yeast strains

The plasmids and bacterial and yeast strains used in this work are listed in Supplementary Table S1. *Escherichia coli* DH5α and *Agrobacterium tumefaciens* GV3101 (Koncz and Schell 1986) were grown on Luria-Bertani agar at 37 and 28°C, respectively. *Pseudomonas fluorescens* was grown on King's B agar at 28°C. Media were supplemented with the appropriate antibiotics when necessary (Supplementary Table S1). *Saccharomyces cerevisiae* strains were grown in 1% yeast extract, 2% peptone, 2% dextrose (YEPD) and synthetic defined (SD) media supplemented with the appropriate amino acids at 30°C (Supplementary Table S1). Plasmids were introduced into *E. coli*, *A. tumefaciens*, and *P. fluorescens* by electroporation as previously described by Shubeita et al. (1987).

Plant material and selection of homozygous mutants

Arabidopsis thaliana Col-0 and T-DNA mutant plants were grown in a plant growth chamber at 23°C with 8 h of light and 50% humidity. *N. tabacum* cultivar Xanthi and *N. benthamiana* plants were grown with a photoperiod of 12 h of light at 24°C. T-DNA insertional mutant SAIL_245_H06 (Sessions et al. 2002) (hereafter *atp23-1*) was obtained from the Arabidopsis Biological Resource Center. The zygosity of mutant plants was confirmed by PCR amplification as described for T-DNA insertions (Li et al. 2007).

Transformation of T-DNA mutants

A. tumefaciens GV3101 strains carrying pCAMBIA1305.2:*Mep23-1* or pCAMBIA1305.2:*Atp23-1* T-DNA plasmids (Supplementary Table S1) were used to transform the *atp23-1* mutant. *Mep23-1* and *Atp23-1* are under the control of the 35S promoter and nopaline synthase (NOS) terminator. Transformation of the *atp23-1* mutant was performed through the flower dip method with *A. tumefaciens* as previously described by Zhang et al. (2006). Seeds collected after transformation were surface-sterilized and plated in selection media (1/2× Murashige and Skoog salts, 0.8% [wt/vol] agar, 25 μg ml^{-1} hygromycin). Transformed T0 seedlings were transplanted to soil and grown to the flowering stage to confirm the presence of the sequences of interest by PCR. Quick DNA extraction from leaf tissue for PCR confirmation was performed as described by Edwards et al. (1991). Further experiments involving transformed plants were carried out with T1 and T2 generations.

Cloning procedures

Total RNA from cassava or *A. thaliana* leaves was isolated using the InviTrap Spin Universal RNA Mini Kit (Stratec Biomedical, Birkenfeld, Germany) following the manufacturer's instructions. cDNA synthesis was performed using the iScript Select cDNA Synthesis Kit (Bio-Rad Laboratories, Hercules, CA, U.S.A.). cDNA was amplified by PCR using Pfu DNA polymerase (Invitrogen, Carlsbad, CA, U.S.A.). For cloning in non-Gateway vectors, restriction enzymes and T4 ligase (New England Biolabs, Ipswich, MA, U.S.A.) were used according to the manufacturer's instructions. For Gateway cloning, the coding sequences were cloned into pENTR/D-TOPO (Invitrogen) following the manufacturer's instructions and then subcloned into Gateway destination vectors using Gateway LR Clonase II enzyme mix (Invitrogen) following the manufacturer's instructions. The plasmid constructs used in this study are described in Supplementary Table S1.

Yeast two-hybrid assay

For the yeast two-hybrid screening, a cassava cDNA library (González Almario and López Carrascal 2008) was constructed in the pLAW11 (activation domain, AD) Gateway vector (Cantu et al. 2013). XopAE was cloned into the pLAW10 (DNA-binding domain, BD) Gateway vector. The library DNA and XopAE construct were transformed into *Saccharomyces cerevisiae* strain AH109. Yeast co-transformation with both pLAW10 and pLAW11 vectors was performed using the lithium acetate method (Clontech Laboratories 2008; Gietz and Woods 2002). Transformed yeast colonies were selected on SD media lacking leucine and tryptophan (SD -L-W) to verify both plasmids' presence. Positive interactions were determined in triple dropout SD media lacking leucine, tryptophan, and histidine (SD -L-W-H). Controls with empty vectors were performed to remove false positives or autoactivation.

Co-immunoprecipitation

The XopAE target in cassava (hereafter *Me*p23-1) was cloned into the pSDK2484 vector with a fusion to the 3×Myc tag, and XopAE or XopN was cloned into the pSDK2483 vector with a fusion to the 3×HA tag using the Gateway cloning system. *A. tumefaciens* GV2260 carrying *Me*p23-1-3×Myc was co-inoculated at an OD_{600} of 0.7 in *N. benthamiana* leaves with *A. tumefaciens* GV2260 containing either XopAE-3×HA or XopN-3×HA at an OD_{600} of 1.2 or 0.7, respectively. Leaves were collected 48 h postinoculation (hpi) and ground into a fine powder with liquid nitrogen. Cells were lysed with extraction buffer (50 mM NaCl, 20 mM Tris pH 7.5, 1 mM ethylenediaminetetraacetic acid [EDTA], 0.1% Triton X-100, 10% glycerol, 5 mM dithiothreitol [DTT], 2 mM NaF, 1 mM phenylmethylsulfonyl fluoride [PMSF], 1× protease inhibitor [Roche, Basel, Switzerland]) and centrifuged at 14,000 rpm for 10 min at 4°C. The supernatant was collected and tumbled with Protein G Sepharose beads (GE Healthcare, Chicago, IL, U.S.A.) at 4°C for 30 min to pre-clear the extract. The mixture was then centrifuged at 3,000 × *g* for 1 min at 4°C, and the supernatant was collected. The pre-cleared extract was tumbled with α-Myc agarose beads (Sigma, St. Louis, MO, U.S.A.) at 4°C for 3 h. Beads were washed four times with washing buffer (300 mM NaCl, 20 mM Tris pH 7.5, 1 mM EDTA, 0.1% Triton X-100, 10% glycerol, 5 mM DTT, 2 mM NaF, 1 mM PMSF, 1× protease inhibitor [Roche]), boiled in 2× loading buffer, and then centrifuged at 10,000 rpm for 2 min. The supernatants were then analyzed by western blotting.

Subcellular localization and BiFC assay

For localization, XopAE and *Me*p23-1 were fused to citrine fluorescent protein (vector pSPDK1677:Citrine) and expressed under the control of the 35S promoter and a NOS terminator as previously described (Padmanabhan et al. 2013). *A. tumefaciens* carrying XopAE:Citrine and *Me*p23-1:Citrine were infiltrated at an OD_{600} of 1.2 and 0.7 in leaves of 4-week-old *N. benthamiana* plants. For BiFC, XopAE was fused to the C-terminal portion of citrine fluorescent protein (vector SPDK1794:^{C}Citrine), and *Me*p23-1 was fused to the N-terminal part of citrine (vector SPDK1823:^{N}Citrine). The BiFC fusions expressed under the control of the 35S promoter and a NOS terminator (Lal et al. 2020; Padmanabhan et al. 2013). *A. tumefaciens* with XopAE:^{C}Citrine and *Me*p23-1:^{N}Citrine were co-infiltrated at an OD_{600} of 1.2 and 0.5, respectively, in leaves of 4-week-old *N. benthamiana* plants. A higher OD was used for the construct expressing XopAE because its in planta expression was very inefficient. Leaves were collected 24, 30, 36, and 48 hpi and visualized immediately. Citrine was excited at 488 nm and fluorescence detected between 498 and 525 nm to detect the fluorescence from tagged proteins. All the imaging was performed using a confocal laser scanning microscope (TCS SP8, Leica Microsystems, Wetzlar, Germany).

Protein structure prediction and protein-protein interaction modeling

Using the predicted translation for *Me*p23-1 from the cassava genome, the predicted three-dimensional (3D) structures were obtained from Robetta using a three-track neural network (Baek et al. 2021). For XopAE, the best prediction was obtained from I-TASSER with an estimated score of 0.68 (Roy et al. 2010; Yang et al. 2015; Zhang 2008). The PDB files of the predicted 3D models for XopAE and *Me*p23-1 were used as input and processed using the QuickPrep function implemented in MOE (Molecular Operating Environment, version 2020.0901, Chemical Computing Group, Montreal, Canada). The QuickPrep function of MOE adds hydrogen atoms to the structure by assessing partial charges and protonation states. Then, the XopAE-*Me*p23-1 interaction was modeled using the Protein-Protein Docking tool of MOE. *Me*p23-1 was set as the receptor and XopAE as the ligand molecule (full-length proteins were docked using the default parameters). We then selected the best model retrieved from the docking based on the MOE Docking Score, which is based on the energy of conformed and restoring scores for each pose, where the most negative score is the best ranked. The best-rated pose was used for epitope analysis, where the most organized cluster of interactions (based on the score) was selected to identify which residues of *Me*p23-1 are targeted by XopAE.

Callose deposition assay

Callose deposition assays in *A. thaliana* plants were performed using a *P. fluorescens* system (Guo et al. 2009; Medina et al. 2018). *A. thaliana* plants were syringe-infiltrated with *P. fluorescens* (pLN1965) carrying the pML123 empty vector (which expresses a T3SS but no T3Es) as a positive control for induction of callose deposition, *P. fluorescens* (pLN1965) carrying either pLN615:XopAE or pLN615:XopAO1, or mock infiltrated with 5 mM morpholine ethane sulfonic acid (MES, pH 5.6). Bacterial suspensions were infiltrated at an OD_{600} of 0.01, and leaves were collected at 16 hpi. Leaves were bleached and stained with aniline blue to visualize callose deposits as previously described (Medina et al. 2018). Leaf sections were visualized under a 10× objective in a fluorescence microscope (Nikon Corporation, Minato, Tokyo, Japan), and the number of callose deposits was determined using Fiji software (Schindelin et al. 2012). At least eight fields were observed per leaf, and three were analyzed per treatment. Experiments were repeated at least twice. Significant differences among plants were determined using Kruskal-Wallis and Dunnet tests ($P < 0.05$), providing the data did not show a normal distribution. Statistical analyses were performed using RStudio version 1.1.442 (RStudio, Boston, MA, U.S.A.).

Quantification of ROS

To quantify ROS in plant tissue, *N. tabacum* cultivar Xanthi leaves were infiltrated with *P. fluorescens* (pLN1965, at 2×10^8 CFU ml^{-1} in MES, pH 5.6) carrying pLN615:XopAE and pML123. ROS production was determined 16 h later using previously described procedures (Kobayashi et al. 2007). Chemiluminescence was monitored every 30 s using a photon image processor with a sensitive CCD camera (ARGUS-50 or Aquacosmos 2.5; Hamamatsu Photonics, Shizuoka, Japan).

HR suppression assay

The HR suppression assay was performed as previously described (Guo et al. 2009; Medina et al. 2018). The strain *P. fluorescens* (pHIR11) carrying pML123 was used as a positive control for HR elicitation, as it holds a T3SS and the effector HopA1 from *P. syringae* pv. *syringae*, which is recognized in *N. tabacum* cultivar Xanthi. This strain was mixed with *P. fluorescens* (pLN1965) carrying pLN615:XopAE (each at 1×10^8 CFU ml^{-1} in 5 mM MES, pH 5.6). Three fivefold serial dilutions of the bacterial suspension were infiltrated in *N. tabacum* cultivar Xanthi leaves. HR responses were recorded at 24 hpi (Guo et al. 2009). The experiment was repeated twice.

Acknowledgments

The authors thank John Rathjen and Isabel Saur for technical guidance and fruitful discussions on methods for this manuscript and Natasha Merindol for valuable discussions on bioinformatic predictions.

Literature Cited

Alfano, J. R., Kim, H.-S., Delaney, T. P., and Collmer, A. 1997. Evidence that the *Pseudomonas syringae* pv. *syringae hrp*-linked *hrmA* gene encodes an Avr-like protein that acts in an *hrp*-dependent manner within tobacco cells. Mol. Plant-Microbe Interact. 10:580-588.

Anjanappa, R. B., Mehta, D., Okoniewski, M. J., Szabelska-Beręsewicz, A., Gruissem, W., and Vanderschuren, H. 2018. Molecular insights into *Cassava brown streak virus* susceptibility and resistance by profiling of the early host response. Mol. Plant Pathol. 19:476-489.

Arrieta-Ortiz, M. L., Rodríguez-R, L. M., Pérez-Quintero, Á. L., Poulin, L., Díaz, A. C., Arias Rojas, N., Trujillo, C., Restrepo Benavides, M., Bart, R., Boch, J., Boureau, T., Darrasse, A., David, P., Dugé de Bernonville, T., Fontanilla, P., Gagnevin, L., Guérin, F., Jacques, M.-A., Lauber, E., Lefeuvre, P., Medina, C., Medina, E., Montenegro, N., Muñoz Bodnar, A., Noël, L. D., Ortiz Quiñones, J. F., Osorio, D., Pardo, C., Patil, P. B., Poussier, S., Pruvost, O., Robène-Soustrade, I., Ryan, R. P., Tabima, J., Urrego Morales, O. G., Vernière, C., Carrere, S., Verdier, V., Szurek, B., Restrepo, S., López, C., Koebnik, R., and Bernal, A. 2013. Genomic survey of pathogenicity determinants and VNTR markers in the cassava bacterial pathogen *Xanthomonas axonopodis* pv. *manihotis* strain CIO151. PLoS One 8:e79704.

Austin, M. J., Muskett, P., Kahn, K., Feys, B. J., Jones, J. D. G., and Parker, J. E. 2002. Regulatory role of *SGT1* in early *R* gene-mediated plant defenses. Science 295:2077-2080.

Baek, M., Dimaio, F., Anishchenko, I., Dauparas, J., Ovchinnikov, S., Lee, G. R., Wang, J., Cong, Q., Kinch, L. N., Schaeffer, R. D., Millán, C., Park, H., Adams, C., Glassman, C. R., Degiovanni, A., Pereira, J. H., Rodrigues, A. V., Van Dijk, A. A., Ebrecht, A. C., Opperman, D. J., Sagmeister, T., Buhlheller, C., Pavkov-Keller, T., Rathinaswamy, M. K., Dalwadi, U., Yip, C. K., Burke, J. E., Garcia, K. C., Grishin, N. V., Adams, P. D., Read, R. J., and Baker, D. 2021. Accurate prediction of protein structures and interactions using a three-track neural network. Science 373:871-876.

Bart, R., Cohn, M., Kassen, A., McCallum, E. J., Shybut, M., Petriello, A., Krasileva, K., Dahlbeck, D., Medina, C., Alicai, T., Kumar, L., Moreira, L. M., Neto, J. R., Verdier, V., Santana, M. A., Kositcharoenkul, N., Vanderschuren, H., Gruissem, W., Bernal, A., and Staskawicz, B. J. 2012. High-throughput genomic sequencing of cassava bacterial blight strains identifies conserved effectors to target for durable resistance. Proc. Natl. Acad. Sci. U.S.A. 109:E1972-E1979.

Bernal-Galeano, V., Ochoa, J. C., Trujillo, C., Rache, L., Bernal, A., and López, C. A. 2018. Development of a multiplex nested PCR method for detection of *Xanthomonas axonopodis* pv. *manihotis* in cassava. Trop. Plant Pathol. 43:341-350.

Bittel, P., and Robatzek, S. 2007. Microbe-associated molecular patterns (MAMPs) probe plant immunity. Curr. Opin. Plant Biol. 10:335-341.

Boher, B., and Verdier, V. 1994. Cassava bacterial blight in Africa: The state of knowledge and implications for designing control strategies. Afr. Crop Sci. J. 2:505-509.

Boller, T. 1995. Chemoperception of microbial signals in plant cells. Annu. Rev. Plant Physiol. Plant Mol. Biol. 46:189-214.

Boller, T., and Felix, G. 2009. A renaissance of elicitors: Perception of microbe-associated molecular patterns and danger signals by pattern-recognition receptors. Annu. Rev. Plant Biol. 60:379-406.

Bolton, M. D. 2009. Primary metabolism and plant defense—Fuel for the fire. Mol. Plant-Microbe Interact. 22:487-497.

Botero, D., Monk, J., Rodríguez Cubillos, M. J., Rodríguez Cubillos, A., Restrepo, M., Bernal-Galeano, V., Reyes, A., González Barrios, A., Palsson, B. Ø., Restrepo, S., and Bernal, A. 2020. Genome-scale metabolic model of *Xanthomonas phaseoli* pv. *manihotis*: An approach to elucidate pathogenicity at the metabolic level. Front. Genet. 11: 837.

Boutrot, F., and Zipfel, C. 2017. Function, discovery, and exploitation of plant pattern recognition receptors for broad-spectrum disease resistance. Annu. Rev. Phytopathol. 55:257-286.

Cantu, D., Yang, B., Ruan, R., Li, K., Menzo, V., Fu, D., Chern, M., Ronald, P. C., and Dubcovsky, J. 2013. Comparative analysis of protein-protein interactions in the defense response of rice and wheat. BMC Genomics 14:166.

Caplan, J., Padmanabhan, M., and Dinesh-Kumar, S. P. 2008. Plant NB-LRR immune receptors: From recognition to transcriptional reprogramming. Cell Host Microbe 3:126-135.

Clontech Laboratories. 2008. Yeast Protocols Handbook. https://www.med.upenn.edu/robertsonlab/assets/user-content/documents/yeast-protocols-handbook.pdf

Cui, H., Tsuda, K., and Parker, J. E. 2015. Effector-triggered immunity: From pathogen perception to robust defense. Annu. Rev. Plant Biol. 66:487-511.

D'Alessandro, S. 2013. Biochemical and functional characterization of p23, a regulatory co-chaperone of HSP90 in Arabidopsis. Ph.D. dissertation. Università degli Studi di Padova, Padua, Italy. http://hdl.handle.net/2318/1784665

Dangl, J. L., Horvath, D. M., and Staskawicz, B. J. 2013. Pivoting the plant immune system from dissection to deployment. Science 341:746-751.

Dodds, P. N., and Rathjen, J. P. 2010. Plant immunity: Towards an integrated view of plant–pathogen interactions. Nat. Rev. Genet. 11:539-548.

Dow, M., Newman, M.-A., and von Roepenack, E. 2000. The induction and modulation of plant defense responses by bacterial lipopolysaccharides. Annu. Rev. Phytopathol. 38:241-261.

Edwards, K., Johnstone, C., and Thompson, C. 1991. A simple and rapid method for the preparation of plant genomic DNA for PCR analysis. Nucleic Acids Res. 19:1349.

Eitas, T. K., and Dangl, J. L. 2010. NB-LRR proteins: Pairs, pieces, perception, partners, and pathways. Curr. Opin. Plant Biol. 13:472-477.

Felix, G., Duran, J. D., Volko, S., and Boller, T. 1999. Plants have a sensitive perception system for the most conserved domain of bacterial flagellin. Plant J. 18:265-276.

Felts, S. J., and Toft, D. O. 2003. p23, a simple protein with complex activities. Cell Stress Chaperones 8:108-113.

Flor, H. H. 1971. Current status of the gene-for-gene concept. Annu. Rev. Phytopathol. 9:275-296.

Flores, C., Zarate, C., Triplett, L., Maillot-Lebon, V., Moufid, Y., Kanté, M., Bragard, C., Verdier, V., Gagnevin, L., Szurek, B., and Robène, I. 2019. Development of a duplex-PCR for differential diagnosis of *Xanthomonas phaseoli* pv. *manihotis* and *Xanthomonas cassavae* in cassava (*Manihot esculenta*). Physiol. Mol. Plant Pathol. 105:34-46.

Forafonov, F., Toogun, O. A., Grad, I., Suslova, E., Freeman, B. C., and Picard, D. 2008. p23/Sba1p protects against Hsp90 inhibitors independently of its intrinsic chaperone activity. Mol. Cell. Biol. 28:3446-3456.

Galán, J. E., and Collmer, A. 1999. Type III secretion machines: Bacterial devices for protein delivery into host cells. Science 284:1322-1328.

Garcia-Ranea, J. A., Mirey, G., Camonis, J., and Valencia, A. 2002. p23 and HSP20/α-crystallin proteins define a conserved sequence domain present in other eukaryotic protein families. FEBS Lett. 529:162-167.

Gietz, R. D., and Woods, R. A. 2002. Transformation of yeast by lithium acetate/single-stranded carrier DNA/polyethylene glycol method. Methods Enzymol. 350:87-96.

Gómez-Cano, F., Soto, J., Restrepo, S., Bernal, A., López-Kleine, L., and López, C. E. 2019. Gene co-expression network for *Xanthomonas*-challenged cassava reveals key regulatory elements of immunity processes. Eur. J. Plant Pathol. 153:1083-1104.

González Almario, C., and López Carrascal, C. E. 2008. Cassava cDNA library construction: One tool for biotechnological development of the crop. Acta Biol. Colomb. 13:189-202.

Guo, L.-M., Li, J., He, J., Liu, H., and Zhang, H.-M. 2020. A class I cytosolic HSP20 of rice enhances heat and salt tolerance in different organisms. Sci. Rep. 10:1383.

Guo, M., Tian, F., Wamboldt, Y., and Alfano, J. R. 2009. The majority of the type III effector inventory of *Pseudomonas syringae* pv. *tomato* DC3000 can suppress plant immunity. Mol. Plant-Microbe Interact. 22:1069-1080.

Hueck, C. J. 1998. Type III protein secretion systems in bacterial pathogens of animals and plants. Microbiol. Mol. Biol. Rev. 62:379-433.

Johnson, J. L., Halas, A., and Flom, G. 2007. Nucleotide-dependent interaction of *Saccharomyces cerevisiae* Hsp90 with the cochaperone proteins Sti1, Cpr6, and Sba1. Mol. Cell. Biol. 27:768-776.

Jones, J. D. G., and Dangl, J. L. 2006. The plant immune system. Nature 444:323-329.

Kay, S., and Bonas, U. 2009. How *Xanthomonas* type III effectors manipulate the host plant. Curr. Opin. Microbiol. 12:37-43.

Kerppola, T. K. 2008. Bimolecular fluorescence complementation (BiFC) analysis as a probe of protein interactions in living cells. Annu. Rev. Biophys. 37:465-487.

Kim, J.-G., Park, B. K., Yoo, C.-H., Jeon, E., Oh, J., and Hwang, I. 2003. Characterization of the *Xanthomonas axonopodis* pv. *glycines* Hrp pathogenicity island. J. Bacteriol. 185:3155-3166.

Kobayashi, M., Ohura, I., Kawakita, K., Yokota, N., Fujiwara, M., Shimamoto, K., Doke, N., and Yoshioka, H. 2007. Calcium-dependent protein kinases regulate the production of reactive oxygen species by potato NADPH oxidase. Plant Cell 19:1065-1080.

Koncz, C., and Schell, J. 1986. The promoter of T_L-DNA gene 5 controls the tissue-specific expression of chimaeric genes carried by a novel type of *Agrobacterium* binary vector. Mol. Gen. Genet. 204:383-396.

Kuang, J., Liu, J., Mei, J., Wang, C., Hu, H., Zhang, Y., Sun, M., Ning, X., Xiao, L., and Yang, L. 2017. A Class II small heat shock protein OsHsp18.0 plays positive roles in both biotic and abiotic defense responses in rice. Sci. Rep. 7:11333.

Lal, N. K., Thanasuwat, B., Huang, P.-j., Cavanaugh, K. A., Carter, A., Michelmore, R. W., and Dinesh-Kumar, S. P. 2020. Phytopathogen effectors use multiple mechanisms to manipulate plant autophagy. Cell Host Microbe 28:558-571.

Lambert, W., Koeck, P. J. B., Ahrman, E., Purhonen, P., Cheng, K., Elmlund, D., Hebert, H., and Emanuelsson, C. 2011. Subunit arrangement in the

dodecameric chloroplast small heat shock protein Hsp21. Protein Sci. 20:291-301.
Li, J., Xiang, C.-Y., Yang, J., Chen, J.-P., and Zhang, H.-M. 2015. Interaction of HSP20 with a viral RdRp changes its sub-cellular localization and distribution pattern in plants. Sci. Rep. 5:14016.
Li, Y., Rosso, M. G., Viehoever, P., and Weisshaar, B. 2007. GABI-Kat SimpleSearch: An *Arabidopsis thaliana* T-DNA mutant database with detailed information for confirmed insertions. Nucleic Acids Res. 35:D874-D878.
Lozano, J. C. 1986. Cassava bacterial blight: A manageable disease. Plant Dis. 70:1089-1093.
Maruri-López, I., Figueroa, N. E., Hernández-Sánchez, I. E., and Chodasiewicz, M. 2021. Plant stress granules: Trends and beyond. Front. Plant Sci. 12:722643.
McHale, L., Tan, X., Koehl, P., and Michelmore, R. W. 2006. Plant NBS-LRR proteins: Adaptable guards. Genome Biol. 7:212.
Medina, C. A., Reyes, P. A., Trujillo, C. A., Gonzalez, J. L., Bejarano, D. A., Montenegro, N. A., Jacobs, J. M., Joe, A., Restrepo, S., Alfano, J. R., and Bernal, A. 2018. The role of type III effectors from *Xanthomonas axonopodis* pv. *manihotis* in virulence and suppression of plant immunity. Mol. Plant Pathol. 19:593-606.
Mutka, A. M., Fentress, S. J., Sher, J. W., Berry, J. C., Pretz, C., Nusinow, D. A., and Bart, R. 2016. Quantitative, image-based phenotyping methods provide insight into spatial and temporal dimensions of plant disease. Plant Physiol. 172:650-660.
Ngou, B. P. M., Ahn, H.-K., Ding, P., and Jones, J. D. G. 2021. Mutual potentiation of plant immunity by cell-surface and intracellular receptors. Nature 592:110-115.
Ngou, B. P. M., Ding, P., and Jones, J. D. G. 2022. Thirty years of resistance: Zig-zag through the plant immune system. Plant Cell 34: 1447-1478.
Nicaise, V., Roux, M., and Zipfel, C. 2009. Recent advances in PAMP-triggered immunity against bacteria: Pattern recognition receptors watch over and raise the alarm. Plant Physiol. 150:1638-1647.
Padmanabhan, M. S., Ma, S., Burch-Smith, T. M., Czymmek, K., Huijser, P., and Dinesh-Kumar, S. P. 2013. Novel positive regulatory role for the SPL6 transcription factor in the N TIR-NB-LRR receptor-mediated plant innate immunity. PLoS Pathog. 9:e1003235.
Pearl, L. H., and Prodromou, C. 2006. Structure and mechanism of the Hsp90 molecular chaperone machinery. Annu. Rev. Biochem. 75: 271-294.
Popov, G., Fraiture, M., Brunner, F., and Sessa, G. 2016. Multiple *Xanthomonas euvesicatoria* type III effectors inhibit flg22-triggered immunity. Mol. Plant-Microbe Interact. 29:651-660.
Popov, G., Majhi, B. B., and Sessa, G. 2018. Effector gene *xopAE* of *Xanthomonas euvesicatoria* 85-10 is part of an operon and encodes an E3 ubiquitin ligase. J. Bacteriol. 200:e00104-18.
Roy, A., Kucukural, A., and Zhang, Y. 2010. I-TASSER: A unified platform for automated protein structure and function prediction. Nat. Protoc. 5:725-738.
Ryan, R. P., Vorhölter, F.-J., Potnis, N., Jones, J. B., Van Sluys, M.-A., Bogdanove, A. J., and Dow, J. M. 2011. Pathogenomics of *Xanthomonas*: Understanding bacterium-plant interactions. Nat. Rev. Microbiol. 9:344-355.
Santhanagopalan, I., Degiacomi, M. T., Shepherd, D. A., Hochberg, G. K. A., Benesch, J. L. P., and Vierling, E. 2018. It takes a dimer to tango: Oligomeric small heat shock proteins dissociate to capture substrate. J. Biol. Chem. 293:19511-19521.
Schindelin, J., Arganda-Carreras, I., Frise, E., Kaynig, V., Longair, M., Pietzsch, T., Preibisch, S., Rueden, C., Saalfeld, S., Schmid, B., Tinevez, J.-Y., White, D. J., Hartenstein, V., Eliceiri, K., Tomancak, P., and Cardona, A. 2012. Fiji: An open-source platform for biological-image analysis. Nat. Methods 9:676-682.
Sessions, A., Burke, E., Presting, G., Aux, G., McElver, J., Patton, D., Dietrich, B., Ho, P., Bacwaden, J., Ko, C., Clarke, J. D., Cotton, D., Bullis, D., Snell, J., Miguel, T., Hutchison, D., Kimmerly, B., Mitzel, T., Katagiri, F., Glazebrook, J., Law, M., and Goff, S. A. 2002. A high-throughput Arabidopsis reverse genetics system. Plant Cell 14:2985-2994.
Shubeita, H. E., Sambrook, J. F., and McCormick, A. M. 1987. Molecular cloning and analysis of functional cDNA and genomic clones encoding bovine cellular retinoic acid-binding protein. Proc. Natl. Acad. Sci. U.S.A. 84:5645-5649.
Singer, A. U., Schulze, S., Skarina, T., Xu, X., Cui, H., Eschen-Lippold, L., Egler, M., Srikumar, T., Raught, B., Lee, J., Scheel, D., Savchenko, A., and Bonas, U. 2013. A pathogen type III effector with a novel E3 ubiquitin ligase architecture. PLoS Pathog. 9:e1003121.
Thao, N. P., Chen, L., Nakashima, A., Hara, S.-i., Umemura, K., Takahashi, A., Shirasu, K., Kawasaki, T., and Shimamoto, K. 2007. RAR1 and HSP90 form a complex with Rac/Rop GTPase and function in innate-immune responses in rice. Plant Cell 19:4035-4045.
Timilsina, S., Potnis, N., Newberry, E. A., Liyanapathiranage, P., Iruegas-Bocardo, F., White, F. F., Goss, E. M., and Jones, J. B. 2020. *Xanthomonas* diversity, virulence and plant–pathogen interactions. Nat. Rev. Microbiol. 18:415-427.
Tosoni, K., Costa, A., Sarno, S., D'Alessandro, S., Sparla, F., Pinna, L. A., Zottini, M., and Ruzzene, M. 2011. The p23 co-chaperone protein is a novel substrate of CK2 in *Arabidopsis*. Mol. Cell. Biochem. 356: 245-254.
Üstün, S., and Börnke, F. 2014. Interactions of *Xanthomonas* type-III effector proteins with the plant ubiquitin and ubiquitin-like pathways. Front. Plant Sci. 5:736.
Verdier, V., Restrepo, S., Mosquera, G., Jorge, V., and Lopez, C. 2004. Recent progress in the characterization of molecular determinants in the *Xanthomonas axonopodis* pv. *manihotis*–cassava interaction. Plant Mol. Biol. 56:573-584.
Wang, W., Feng, B., Zhou, J.-M., and Tang, D. 2020. Plant immune signaling: Advancing on two frontiers. J. Integr. Plant Biol. 62:2-24.
White, F. F., Potnis, N., Jones, J. B., and Koebnik, R. 2009. The type III effectors of *Xanthomonas*. Mol. Plant Pathol. 10:749-766.
Yang, J., Yan, R., Roy, A., Xu, D., Poisson, J., and Zhang, Y. 2015. The I-TASSER Suite: Protein structure and function prediction. Nat. Methods 12:7-8.
Zárate-Chaves, C. A., Gómez de la Cruz, D., Verdier, V., López, C. E., Bernal, A., and Szurek, B. 2021a. Cassava diseases caused by *Xanthomonas phaseoli* pv. *manihotis* and *Xanthomonas cassavae*. Mol. Plant Pathol. 22:1520-1537.
Zárate-Chaves, C. A., Osorio-Rodríguez, D., Mora, R. E., Pérez-Quintero, Á. L., Dereeper, A., Restrepo, S., López, C. E., Szurek, B., and Bernal, A. 2021b. TAL effector repertoires of strains of *Xanthomonas phaseoli* pv. *manihotis* in commercial cassava crops reveal high diversity at the country scale. Microorganisms 9:315.
Zhang, X., Henriques, R., Lin, S.-S., Niu, Q.-W., and Chua, N.-H. 2006. *Agrobacterium*-mediated transformation of *Arabidopsis thaliana* using the floral dip method. Nat. Protoc. 1:641-646.
Zhang, Y. 2008. I-TASSER server for protein 3D structure prediction. BMC Bioinform. 9:40.
Zhang, Z., Sullivan, W., Felts, S. J., Prasad, B. D., Toft, D. O., and Krishna, P. 2010. Characterization of plant p23-like proteins for their co-chaperone activities. Cell Stress Chaperones 15:703-715.
Zipfel, C. 2009. Early molecular events in PAMP-triggered immunity. Curr. Opin. Plant Biol. 12:414-420.
Zipfel, C., and Robatzek, S. 2010. Pathogen-associated molecular pattern-triggered immunity: Veni, vidi...? Plant Physiol. 154:551-554.
Zipfel, C., Robatzek, S., Navarro, L., Oakeley, E. J., Jones, J. D. G., Felix, G., and Boller, T. 2004. Bacterial disease resistance in *Arabidopsis* through flagellin perception. Nature 428:764-767.